ACS OMEGA

http://pubs.acs.org/journal/acsodf

Article

Electronic Properties and Electrocatalytic Water Splitting Activity for Precious-Metal-Adsorbed Silicene with Nonmetal Doping

Wen-Zhong Li, Yao He,* Yong Mao, and Kai Xiong

Cite This: *ACS Omega* 2022, 7, 33156−33166

Read Online

ACCESS | Metrics & More | Article Recommendations | Supporting Information

ABSTRACT: Since nonmetal (NM)-doped two-dimensional (2D) materials can effectively modulate their physical properties and chemical activities, they have received a lot of attention from researchers. Therefore, the stability, electronic properties, and electrocatalytic water splitting activity of precious-metal (PM)-adsorbed silicene doped with two NM atoms are investigated based on density functional theory (DFT) in this paper. The results show that NM doping can effectively improve the stability of PM-adsorbed silicene and exhibit rich electronic properties. Meanwhile, by comparing the free energies of the hydrogen evolution reaction (HER) and oxygen evolution reaction (OER) intermediates of 15 more stable NM-doped systems, it can be concluded that the electrocatalytic water splitting activity of the NM-doped systems is more influenced by the temperature. Moreover, the Si−S2−Ir-doped system exhibits good HER performance when the temperature is 300 K, while the Si−N2−Pt-doped system shows excellent OER activity. Our theoretical study shows that NM doping can effectively promote the stability and electrocatalytic water splitting of PM-adsorbed silicene, which can help in the application of silicene in electrocatalytic water splitting.

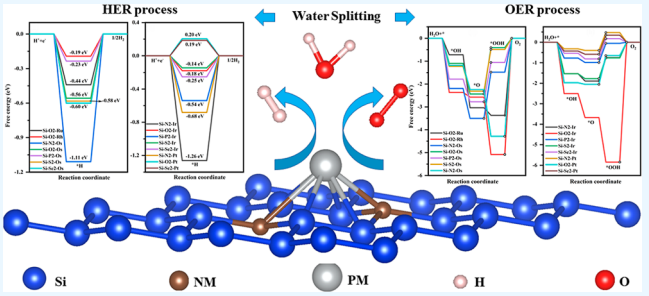

1. INTRODUCTION

Hydrogen production by water electrolysis has been considered by researchers and industries as a simple and nonpolluting method to mitigate the energy crisis, but its application is limited by the low conversion efficiency of electrolytic water.[1−3] Water electrolysis consists of oxygen evolution reaction (OER) at the anode[4] and hydrogen evolution reaction (HER) at the cathode.[5] Therefore, the use of cathode and anode materials with strong stability and high reactivity is a prerequisite to guarantee the increased conversion efficiency of hydrogen production from electrolytic water. In addition, from the kinetic point of view, the OER process of the anode is slow, which can hinder the whole water electrolysis process.[4,6−9] Therefore, the search for catalysts with high electrolytic water reaction activity has become an urgent problem.

In recent years, two-dimensional (2D) materials have attracted much attention in catalysis and other fields due to their unique structure and electronic properties.[10−13] Graphene and its derivatives[9,14−23] and monolayer transition-metal chalcogenides (TMCs)[24−32] are the more widely used two-dimensional materials in the field of electrocatalysis. For example, due to the low electrochemical activity of graphene, graphene can be made better electrochemically active by defect engineering[33−35] and using dopant[36−39] and functional groups[40,41] that can modulate the electronic states at the Fermi energy level. In contrast to graphene, the derivatives of graphene have abundant electronic states and strong stability, which are often used in electrocatalytic reactions.[12] For example, Qiao et al.[42,43] combined g-C3N4 and N-doped graphene to render this composite material with strong stability and high activity for the HER. However, TMCs can be directly used in some catalytic reactions, and also, their electronic properties and catalytic activity can be regulated by methods of surface modification[44−48] and introduction of defects.[49,50] For example, a single-layer WS_2 nanosheet exhibits excellent activity for the HER,[32] while single-layer MoS_2 is required to improve the electrocatalytic reaction performance by some methods, such as doping and defect engineering.[26,28,29,45−49]

Doped silicene has been attracting immense interest from researchers due to its rich physical properties and chemical activity. For example, Ni-doped silicene has high stability and magnetic properties of a certain size.[51] Fe- and Cr-doped silicene has rich magnetic properties.[52−54] Pd-, Pt-, and Au-adsorbed silicene has high stability and rich electronic properties.[55] Meanwhile, silicene-supported Pt was used for the CO oxidation reaction,[56] while Ru-, Rh-, and Ir-adsorbed

Received: May 31, 2022
Accepted: July 11, 2022
Published: September 6, 2022

https://doi.org/10.1021/acsomega.2c03388
ACS Omega 2022, 7, 33156−33166

silicene has strong stability and excellent HER properties.[57] In addition, nonmetal (NM) doping can also modulate the electronic properties of silicene to give it a high chemical activity. For example, B-doped silicene nanoribbons can be changed from a semiconductor to metal, resulting in enhanced conductivity.[58] P-substituted doped silicene can improve the stability of silicene.[59] The theoretical study of Jose and Datta[60,61] revealed the microscopic origin of buckling deformation in silicene, and Li ions can inhibit the short-range puckering in silicene, thus opening up the band gap. $CaSi_2$,[62] a layered material formed by Ca ions and silicene, has perfect planar silicene layers and shows Dirac cones at high symmetry points K and H. B and N doping can improve the stability and sensitivity of silicene to NO and NO_2 gases, which helps in the application of silicene in gas sensors.[63] Moreover, siloxene is an oxide of silicene, which has high selectivity and electrochemical activity.[64] This shows that NM or transition-metal (TM)-doped silicene has strong stability and good chemical reactivity. Therefore, in this paper, we try to introduce NMs and precious metals (PMs) to induce NMs and PMs to form compounds on the silicene surface to obtain higher stability and to investigate their electronic properties and electrolytic water activity.

In previous studies, we have investigated the stability and electronic properties of PM-adsorbed silicene and confirmed that PMs adsorbed on the silicene surface at the H-site are the most stable and exhibit a good water splitting activity.[57] Therefore, in this paper, the theoretical approach of first principles was applied to study the stability, electronic properties, and water splitting activity of PM (PM = Ru, Rh, Pd, Ag, Os, Ir, Pt, Au)-adsorbed silicenes by doping them with two NMs (NM = C, N, O, P, S, Se) atoms, labeled Si−(NM)2−PM (see Figure 1). By comparing the binding energies of 48 NM-doped systems, it can be found that NM doping can effectively improve the stability of PM-adsorbed silicene. Then, we systematically studied the electronic properties of 15 more stable NM-doped systems and analyzed the magnetic properties of the stable systems. Finally, by comparing the free-energy changes of the HER and OER intermediates, we can conclude that the HER and OER activities of the NM-doped systems are influenced by temperature. Also, when the temperature is 300 K, the Si−S2−Ir-doped system has excellent HER performance, while the Si−N2−Pt-doped system has the best OER activity. It can be seen that NM doping can not only effectively improve the stability of PM-adsorbed silicene but also has good electrocatalytic water splitting activity, which provides a theoretical basis for the application of silicene in electrocatalysis.

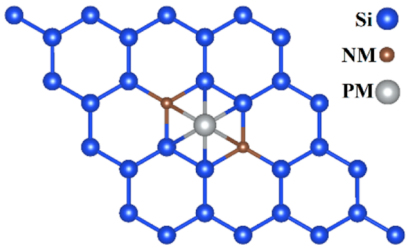

Figure 1. Geometrical structure of silicene-supported PMs with doped NMs.

2. METHODS AND COMPUTATIONAL DETAILS

Our study was based on the spin density functional theory (DFT),[65,66] and the theoretical simulation calculations were carried out by using the Vienna ab initio simulation package (VASP) code.[67,68] The projector augmented wave method was used to describe the interaction between electrons and ions.[69] The exchange−correlation functional type is Perdew−Burke−Ernzerhof (PBE) within the generalized gradient approximation.[70] The kinetic energy cutoff value of all simulation calculations was set to 500 eV, the energy convergence accuracy of electrons was set to 1×10^{-6} eV, and the convergence accuracy of atomic force was set to 0.02 eV/Å in structural optimization. A $3 \times 3 \times 1$ Monkhorst−Pack grid was used in the Brillouin zone for structural optimization, and a $7 \times 7 \times 1$ Monkhorst−Pack grid was used for static calculations. The structural model used in the calculations was based on the structural model of PMs (PM = Ru, Rh, Pd, Ag, Os, Ir, Pt, Au) adsorbed on the $4 \times 4 \times 1$ silicene surface supercell at the H-site, in which two NM (NM = C, N, O, P, S, Se) atoms were doped (see Figure 1), labeled Si−(NM)2−PM. In order to eliminate the interaction between adjacent carriers, the vacuum layer thickness was set to 20 Å. In addition, this study also used the VASPKIT[71] code and VESTA[72] software to process the data and display the results. Due to the strong correlation effect of d-electrons in TMs, the accurate simulation of related properties may be affected. Therefore, the DFT + U methods[73] were used to modify the results in this paper. The Hubbard-U values used in the calculations were obtained by the linear response methods of Cococcioni and de Gironcoli[74] (the calculation method and results are shown in the Supporting Information, Figures S1−S8 and Table S1).

The electrocatalytic water splitting process includes the HER at the cathode and the OER at the anode. In general, the HER process in an acidic environment is as follows[5]

$$* + H^+ + e^- \rightarrow {}^*H \tag{1}$$

$${}^*H + H^+ + e^- \rightarrow H_2 \tag{2}$$

where * and *H represent active sites on the surface of the support and HER intermediate, respectively. However, the OER needs to be a $4e^-$ process[4]

$$* + H_2O(l) \rightleftharpoons {}^*OH + H^+ + e^- \tag{3}$$

$${}^*OH \rightleftharpoons {}^*O + H^+ + e^- \tag{4}$$

$${}^*O + H_2O(l) \rightleftharpoons {}^*OOH + H^+ + e^- \tag{5}$$

$${}^*OOH \rightleftharpoons {}^* + O_2 + H^+ + e^- \tag{6}$$

where *OH, *O, and *OOH represent three OER intermediates. Moreover, all calculations of electrocatalytic performance were based on the standard hydrogen electrode (SHE) in the acidic medium.

The calculation formulas involved in this paper are as follows

$$E_b = E_{Si-(NM)2} + E_{PM} - E_{Si-(NM)2-PM} \tag{7}$$

$$E_{ads-*H} = E_{Si-(NM)2-PM} + \frac{1}{2}E_{H_2} - E_{*H} \tag{8}$$

$$\Delta G = \Delta E + \Delta E_{ZPE} - T\Delta S \tag{9}$$

https://doi.org/10.1021/acsomega.2c03388
ACS Omega 2022, 7, 33156−33166

Equations 7−9 are the calculated equations of binding energy for NM-doped systems (E_b),[75] adsorption energy for the HER intermediate ($E_{ads\text{-}*H}$),[57,75,76] and adsorption free energy for the reaction intermediates (ΔG),[5] respectively, where $E_{Si-(NM)2}$, E_{PM}, $E_{Si-(NM)2-PM}$, E_{H_2}, and E_{*H} are the total energies of NM-doped silicene, single PM atom, Si−(NM)2−PM-doped systems, H_2, and *H, respectively. Moreover, ΔE, ΔE_{ZPE}, T, and ΔS are the reaction intermediates' chemisorption energy, reaction zero-point energy, environment temperature, and entropy changes between the adsorbed and the gas phase, respectively.

3. RESULTS AND DISCUSSION

3.1. Stability and Electronic Properties. Our previous studies have found that PM-adsorbed silicenes at the H-site are the most stable.[57] Hence, in this paper, we doped two NM atoms (as shown in Figure 1) in the PM-adsorbed silicene to study its stability and electronic properties. It can be seen in Table 1 that NM doping can effectively improve the stability of PM-adsorbed silicene.[57] For instance, the binding energy of the O2-doped Os adsorption system (Si−O2−Os) increases by about 3.17 eV compared to Os-adsorbed silicene,[57] which suggests that O2 doping can significantly improve the stability of Os-adsorbed silicene. In terms of the magnitude of the binding energy, the O2-doped systems are the most stable compared to other NM-doped systems; meanwhile, NM doping provides greater stability for Os-, Ir-, and Pt-adsorbed silicene. At the same time, it can be seen in Figure 2 that the binding energies of most NM-doped systems are higher than 1 eV, which implies that NM doping is beneficial to improve the stability of PM-adsorbed silicene. Among them, the number of NM-doped systems with a binding energy from 4 to 5 eV is the highest, and there are 15 kinds of doped systems whose binding energy exceeds 5 eV, which provides a great possibility for the application of silicene-supported PM with NM doping. Compared with the stability of TM-doped silicene[52,55] and germanene,[77,78] the stability of PM-adsorbed silicene with doped NMs is obviously improved. Therefore, we choose more stable doped systems as the main objects of this paper, namely, Si−O2−Ru, Si−O2−Rh, Si−N2−Os, Si−O2−Os, Si−P2−Os, Si−S2−Os, Si−Se2−Os, Si−N2−Ir, Si−O2−Ir, Si−P2−Ir, Si−S2− Ir, Si−Se2−Ir, Si−N2−Pt, Si−O2−Pt, and Si−Se2−Pt for a total of 15 doped systems. Moreover, it can be observed in Table 1 that the stability of the N2-, O2-, and S2-doped systems decreases with increasing atomic number of PM in the PM adsorption systems within the same period. For example, the binding energy of Si−O2−Ru-, Si−O2−Rh-, Si−O2−Pd-, and Si−O2−Ag-doped systems decreases with increasing atomic number of the PM, which reveals that the stability of O2-doped systems decreases with increasing atomic number of PMs in the PM adsorption systems within the same period.

Table 1. Binding Energy (E_b) of Silicene-Supported PMs with Doped NMs

	E_b (eV)					
	C2	N2	O2	P2	S2	Se2
Ru	2.91	4.43	6.05	3.63	3.91	4.21
Rh	2.97	4.14	5.86	3.62	3.88	4.15
Pd	2.98	3.46	4.51	3.40	3.22	3.15
Ag	0.67	1.23	1.79	1.33	1.72	1.77
Os	4.13	6.48	7.83	5.12	6.43	6.20
Ir	4.70	6.27	7.72	5.61	5.76	6.30
Pt	4.25	5.14	7.70	4.80	4.80	5.41
Au	0.99	1.42	2.59	1.58	1.97	2.05

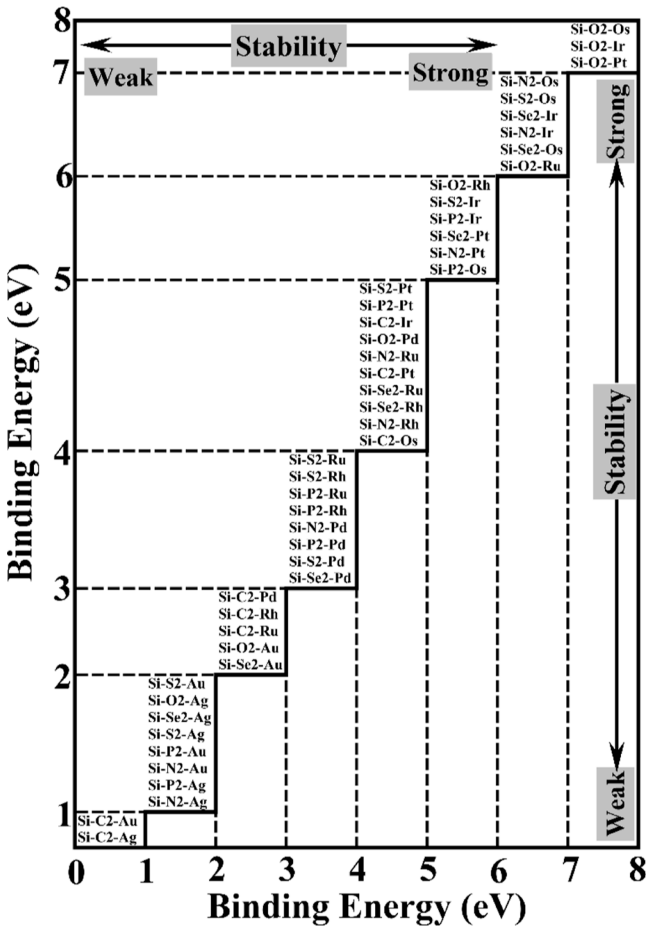

Figure 2. Schematic diagram of stability strength for silicene-supported PMs with doped NMs.

Figures S9−S12 show the geometrical structures and some of the structural parameters of the 15 more stable NM-doped systems. In Figures S9−S12, it can be seen that the geometrical structures of the Si−(NM)2−PM systems are dramatically different from those of pristine silicene[79] and PM-adsorbed silicene.[57] In particular, compared with the geometry of pristine silicene,[79] the 15 NM-doped systems have undergone a large deformation within the surface, but the bond length between the Si atoms at the edges of the Si−(NM)2−PM systems remains about 2.27 Å, so the buckled height between the edge Si atoms remains around 0.44 Å. For example, it can be seen in Figures S9c, S10a,d, and S12a that the Si−N2−Os, Si−P2−Os, Si−N2−Ir, and Si−N2−Pt systems are less deformed compared to the geometries of PM-adsorbed silicene, and their geometries are similar to those of PM-adsorbed silicene[57] (i.e., the NM and Si atoms near the PM still can form a complete hexagon); meanwhile, Si−O2−Ru, Si−O2−Rh, Si−O2−Os, Si−O2−Ir, and Si−O2−Pt (see Figures S9a,b,d, S11a,b, respectively) have similar geometries and two O atoms are not involved in supporting the PM atoms. In addition, the Pt atom migrates from the H-site to V-site in the Si−Se2−Pt system (i.e., above the Se atom, see Figure S12c) compared to before and after structural

https://doi.org/10.1021/acsomega.2c03388
ACS Omega 2022, 7, 33156−33166

optimization, which indicates that the Pt atom is stably anchored on the Se atom.

To study the interaction between the PM atom and the nearest atoms, we calculated the charge transfer and charge density difference for each of the 15 NM-doped systems in Table 2 and Figures S13 and S14. It can be seen in Table 2 that the PM atoms obtain electrons from other atoms in the Si−(NM)2−PM-doped systems. For example, 0.25 e is transferred to the Ru atom in the Si−O2−Ru-doped system, which is opposite to the charge-transfer situations of Ru-adsorbed silicene.[57] It can also be seen in Table 2 that the charge-transfer situations of other NM-doped systems are the same as that of PM-adsorbed silicene[57] except for the Si−O2−Ru-doped system, but their charge-transfer numbers are different. For example, the Os atom gets 0.23 e from other atoms in the Si−N2−Os-doped system, and the charge-transfer number of the Si−N2−Os-doped system increases by 0.09 e compared with that of Os-adsorbed silicene.[57] It can be seen in Figures S13 and S14 that the charge accumulation of the NM-doped systems, except for the Si−N2−Os-doped system, is from the depleted charge of the PM to the accumulated charge between atoms and to the depleted charge of the nearest atoms to PM, and their charge accumulation is similar to that of PM-adsorbed silicene.[57] Based on the charge-transfer situations and charge density difference, it can be tentatively inferred that ionic interactions exist between the PM atom and the neighboring atoms.

Table 2. Charge Transfer (Δq), Energy Band Gap (E_g), and Total Magnetic Moments (M_t) of 15 PM-Adsorbed Silicenes with Doped NMs [Si−(NM)2−PM][a]

	Δq (e)	E_g (eV)	M_t (μ_B)	M_{Si} (μ_B)	M_{NM} (μ_B)	M_{PM} (μ_B)
Si−O2−Ru	0.25	0.04	0			
Si−O2−Rh	0.52	m	0.30	0.24	0.01	0.05
Si−N2−Os	0.23	0.08	0			
Si−O2−Os	0.68	m	0			
Si−P2−Os	0.52	0.20	0			
Si−S2−Os	0.05	m	0			
Si−Se2−Os	0.17	m	0			
Si−N2−Ir	0.12	m	0			
Si−O2−Ir	0.12	m	0			
Si−P2−Ir	0.30	m	0			
Si−S2−Ir	0.34	m	0.37	0.29	0.05	0.03
Si−Se2−Ir	0.18	m	0.79	0.64	0.03	0.12
Si−N2−Pt	0.53	m	0			
Si−O2−Pt	0.48	0.09	0			
Si−Se2−Pt	0.76	m	0			

[a] M_{Si}, M_{NM}, and M_{PM} represent all Si magnetic moments, two NM atoms' magnetic moment, and PM atomic magnetic moment. "m" stands for metallic.

To investigate the electronic properties of the 15 Si−(NM)2−PM-doped systems, we display their total density of states (TDOS) in Figures 5 and 6. In Figures 5 and 6, it can be found that the Si−O2−Ru-, Si−N2−Os-, Si−P2−Os-, and Si−O2−Pt-doped systems exhibit semiconducting properties with narrow energy gaps (see Table 2 for band gap values), while other NM-doped systems exhibit metallic properties. For example, it can be observed in Figure 5 that the Si−N2−Ir-doped system has active electrons at the Fermi energy level, which indicates that Si−N2−Ir exhibits metallic properties,

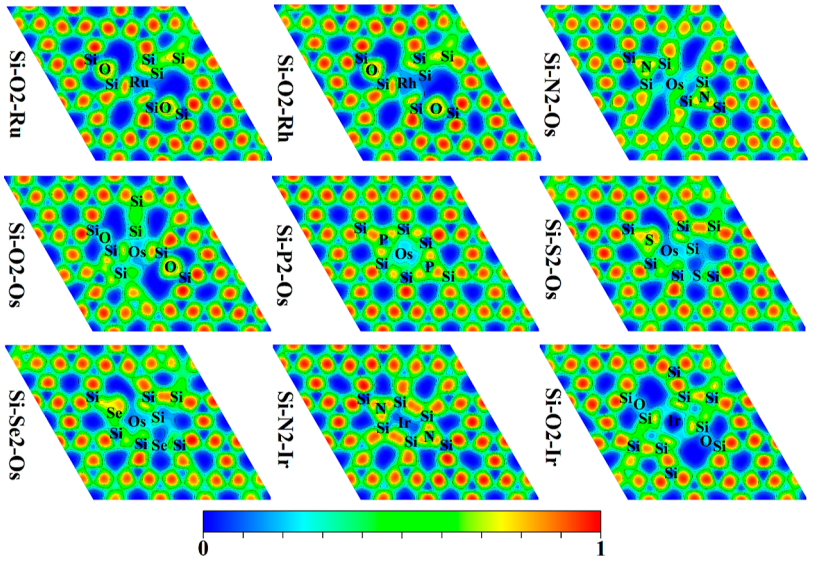

Figure 3. ELF of Si−O2−Ru, Si−O2−Rh, Si−N2−Os, Si−O2−Os, Si−P2−Os, Si−S2−Os, Si−Se2−Os, Si−N2−Ir, and Si−O2−Ir.

https://doi.org/10.1021/acsomega.2c03388
ACS Omega 2022, 7, 33156−33166

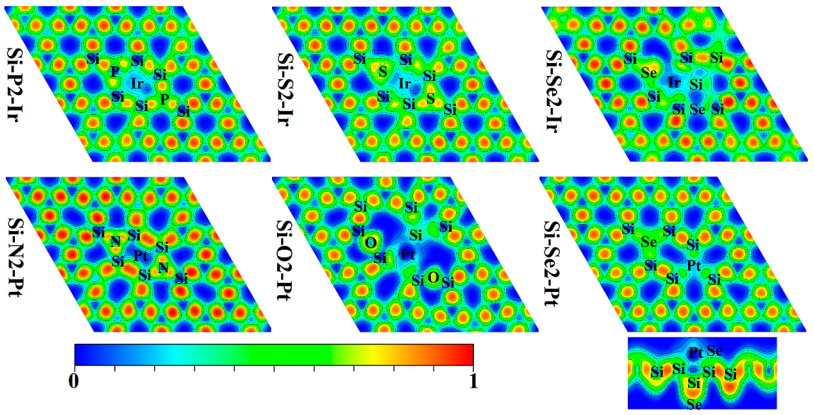

Figure 4. ELF of Si−P2−Ir, Si−S2−Ir, Si−Se2−Ir, Si−N2−Pt, Si−O2−Pt, and Si−Se2−Pt.

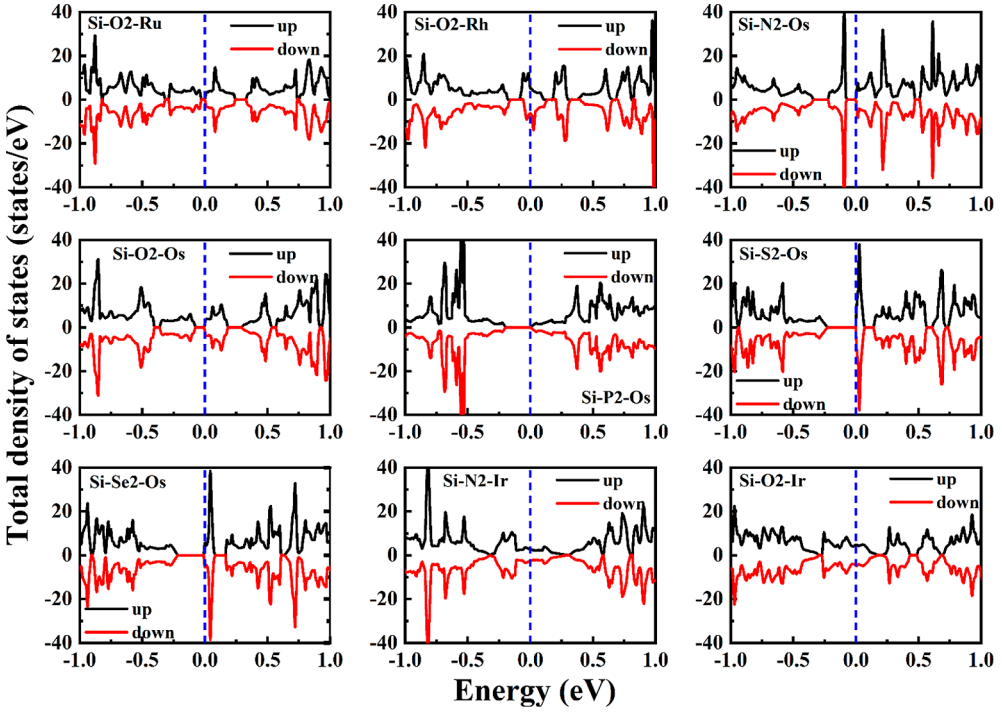

Figure 5. TDOS of Si−O2−Ru, Si−O2−Rh, Si−N2−Os, Si−O2−Os, Si−P2−Os, Si−S2−Os, Si−Se2−Os, Si−N2−Ir, and Si−O2−Ir.

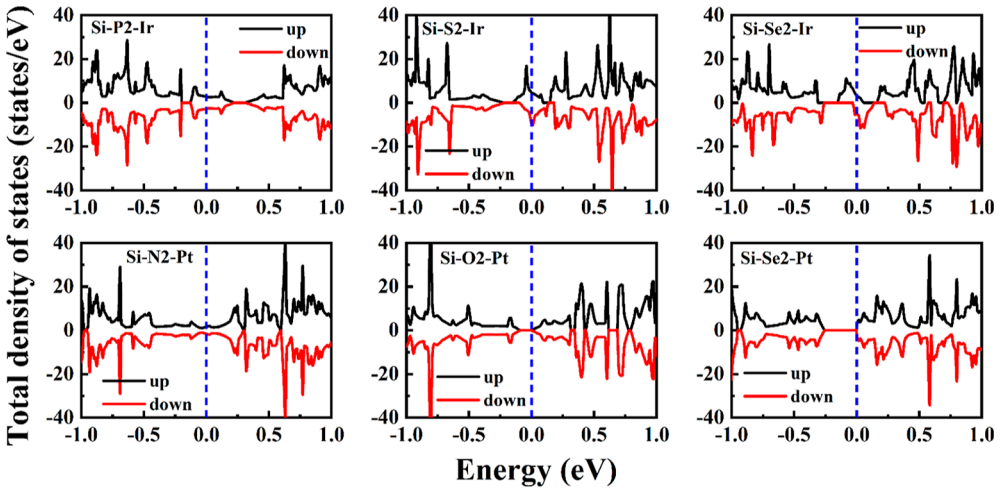

Figure 6. TDOS of Si−P2−Ir, Si−S2−Ir, Si−Se2−Ir, Si−N2−Pt, Si−O2−Pt, and Si−Se2−Pt.

https://doi.org/10.1021/acsomega.2c03388
ACS Omega 2022, 7, 33156−33166

and metallic conductors are favorable for electron transport for electrocatalytic reactions. Furthermore, it can be seen in Table 2 that the band gap values of Si−O2−Ru-, Si−N2−Os-, Si−P2−Os-, and Si−O2−Pt-doped systems are significantly decreased compared to those of Ru-,[57] Os-,[57] Pt-,[57] and Fe-adsorbed silicene,[52] which indicates that NM doping can improve the conductivity of PM- and TM-adsorbed silicenes.

Figures S15−S18 show the projected density of states (PDOS) of the 15 NM-doped systems. From their orbital PDOS, it can be observed that there are different degrees of orbital hybridization between Si-p orbitals and PM-d orbitals in the 15 NM-doped systems, which implies that there are interactions between Si-p orbitals and PM-d orbitals. For example, the strong orbital hybridization between Si-p orbitals and Rh-d orbitals in the Si−O2−Rh-doped system suggests that there may be a strong interaction between Si and PMs; this phenomenon may occur because of the existence of ionic and covalent bonding interactions between the Rh atom and the nearest Si atoms. Meanwhile, except for the Si−O2−PM-doped system, the PM-d orbitals and NM-p orbitals have different degrees of orbital hybridization in other NM-doped systems. In addition, the PM-d orbitals have active electrons near the Fermi energy level in the other NM-doped systems besides Si−O2−Ru-, Si−N2−Os-, Si−P2−Os-, and Si−O2−Pt-doped systems, which can help oxygen molecules to obtain higher chemical reactivity.[80]

In order to study the magnetic properties of the 15 NM-doped systems, we calculated the total magnetic moments (M_t) of Si−(NM)2−PM, as shown in Table 2. It can be found that the Si−O2−Rh-, Si−S2−Ir-, and Si−Se2−Ir-doped systems have magnetic moments of a certain magnitude, while the magnetic moments of other NM-doped systems are 0, which means that Si−O2−Rh-, Si−S2−Ir-, and Si−Se2−Ir-doped systems are magnetic, while other NM-doped systems are nonmagnetic. The magnetic properties of the doped systems are due to the fact that the spin-up electronic states and the spin-down electronic states are asymmetric (see Figures 5 and 6). To further determine the magnetic contributions of Si−O2−Rh-, Si−S2−Ir-, and Si−Se2−Ir-doped systems, the total magnetic moments of all Si (M_{Si}) and two NM atoms (M_{NM}) and the magnetic moments (M_{PM}) of the PM atom are given in Table 2. It can be seen in Table 2 that the total magnetic moments of all Si atoms are the largest in the Si−O2−Rh-, Si−S2−Ir-, and Si−Se2−Ir-doped systems compared to the magnetic moments of other atoms, which means that all Si atoms contribute the most to the magnetism in the Si−O2−Rh-, Si−S2−Ir-, and Si−Se2−Ir-doped systems. For example, the total magnetic moment of the Si−Se2−Ir-doped system is 0.79 μ_B, while the total magnetic moment of all Si atoms in the Si−Se2−Ir-doped system is 0.64 μ_B, which indicates that the magnetic properties of the Si−Se2−Ir-doped system mainly originate from all Si atoms. In addition, O2 doping can make Rh- and Ir-adsorbed silicene become magnetic compared to Rh- and Ir-adsorbed silicene,[57] while S2 and Se2 doping can make Ir-adsorbed silicene magnetic.

3.2. Electrocatalytic Water Splitting Activity. In order to study the HER activity of 15 more stable NM-doped systems, we calculated the free energy variation of the HER at temperatures between 200 and 600 K, as shown in Figure 7. In Figure 7, it can be observed that the free energy of HER intermediates (*H) shows an increasing trend in the NM-doped systems. Among them, the free energy of *H of Si−O2−Pt- and Si−Se2−Pt-doped systems increases with

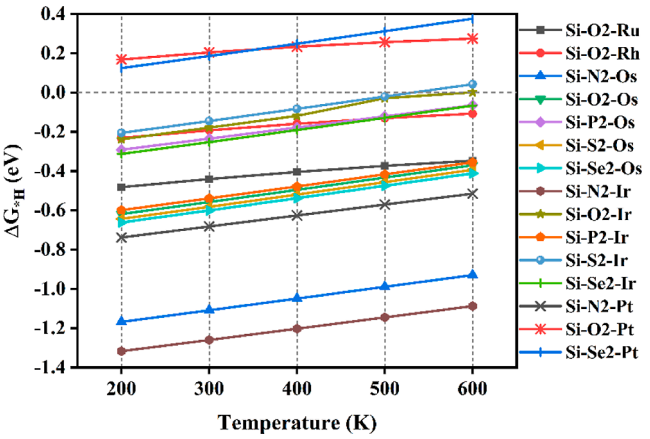

Figure 7. Free-energy changes of HER intermediates (*H) at temperatures between 200 and 600 K.

increasing temperature, which means that the HER activity of Si−O2−Pt- and Si−Se2−Pt-doped systems decreases with increasing temperature. However, since the free-energy values of HER intermediates (*H) of other NM-doped systems are negative values except for Si−O2−Pt- and Si−Se2−Pt-doped systems, the free energy of their HER intermediates (*H) increases with increasing temperature, which means that the HER performance of the NM-doped systems increases with increasing temperature except for Si−O2−Pt- and Si−Se2−Pt-doped systems. Furthermore, it can also be seen in Figure 7 that the free energy of *H of Si−O2−Rh-, Si−P2−Os-, Si−O2−Ir-, Si−S2−Ir-, and SiSe2−Ir-doped systems tends to exceed 0. It can be inferred that the HER activity of Si−O2−Rh-, Si−P2−Os-, Si−O2−Ir-, Si−S2−Ir-, and SiSe2−Ir-doped systems may decrease at higher temperatures.

Figure 8 presents the HER free-energy diagram at a temperature of 300 K. In Figure 8, it can be seen that the free-energy change of *H of the Si−S2−Ir-doped system is the closest to 0 while that of the Si−N2−Ir-doped system is the furthest away from 0, which means that the HER performance of the Si−S2−Ir-doped system is the best while that of Si−N2−Ir-doped system is the worst. In addition, compared with the hydrogen evolution activity of Ir-adsorbed silicene,[56] the hydrogen evolution activity of Ir-adsorbed silicene was obviously enhanced by S2 doping. From Figure 8, it can also be concluded that the hydrogen evolution activities of Si−O2−Rh- and Si−Se2−Pt-doped systems are the same, but their free-energy values differ by a negative sign, implying that the rate-determining step (RDS) of the Si−O2−Rh-doped system occurs during the desorption process of hydrogen evolution intermediates (*H) to generate hydrogen (H_2) while that of the Si−Se2−Pt-doped system occurs during the adsorption process of hydrogen ions on the surface of the support to generate *H. Furthermore, Figure 9 exhibits the plot between the free energy of the HER intermediate (*H) and the adsorption energy of *H. A linear decreasing relationship between the free energy of *H and the adsorption energy of *H can be seen in Figure 9, implying that the HER activity of the NM-doped systems decreases as the adsorption energy of the HER intermediate (*H) increases. This result is similar to the findings of Nørskov et al.[5]

The limiting reaction barrier (ΔG_{RDS}) is an important parameter to evaluate the OER activity, which is determined by the RDS.[4,9,14] To understand the electrocatalytic oxygen

https://doi.org/10.1021/acsomega.2c03388
ACS Omega 2022, 7, 33156−33166

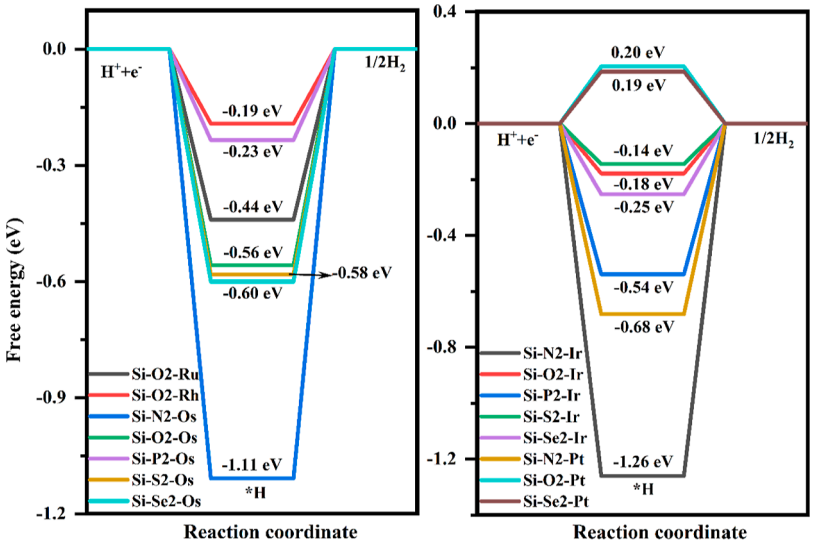

Figure 8. Free-energy diagram of HER intermediates (*H) at 300 K.

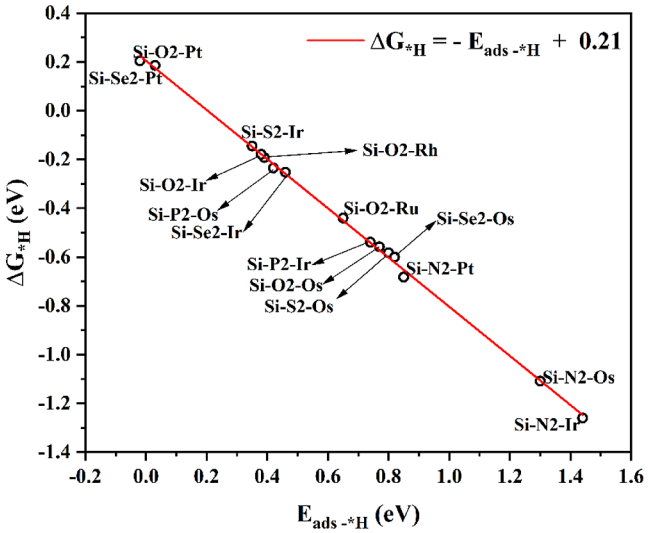

Figure 9. Linear fit between HER intermediates' free-energy changes (ΔG_{*H}) and HER intermediates' adsorption energy ($E_{ads\text{-}*H}$).

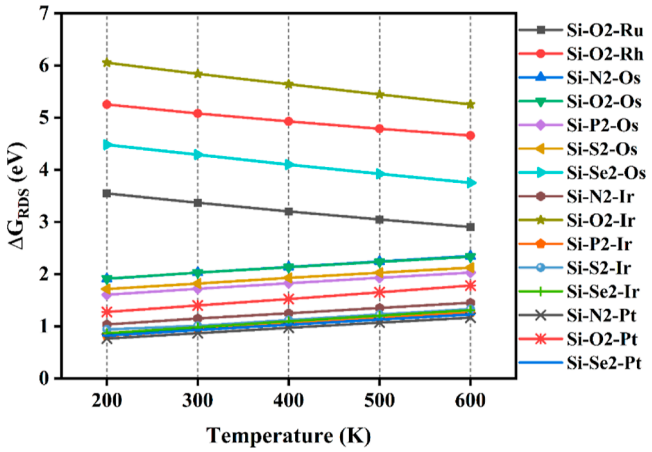

Figure 10. Limiting reaction barrier (ΔG_{RDS}) of the OER at temperatures between 200 and 600 K.

evolution performance of the 15 NM-doped systems, we calculated the limiting reaction barrier (ΔG_{RDS}) at 1.23 eV for the OER at different temperatures (200−600 K), as shown in Figure 10. In Figure 10, it can be seen that the limiting reaction barrier (ΔG_{RDS}) of Si−O2−Ir-, Si−O2−Rh-, Si−Se2−Os-, and Si−O2−Ru-doped systems decreases with increasing temperature, while that of other doped systems increases with increasing temperature, implying that the OER activity of the Si−O2−Ir-, Si−O2−Rh-, Si−Se2−Os-, and Si−O2−Ru-doped systems is enhanced with increasing temperature, whereas the oxygen evolution performance of other doped systems decreases with increasing temperature. Moreover, it can be found in Tables S2 and S3 that, except for the Si−S2−Ir-doped system, the RDS of the OER is not affected by temperature in other NM-doped systems. For example, the RDS of the OER in the Si−N2−Pt-, Si−O2−Pt-, and Si−Se2−Pt-doped systems is not affected by temperature and is always *O → *OOH.

Figure 11 and Table 3 show the free energy, RDS, and the limiting reaction barrier (ΔG_{RDS}) at 1.23 eV for the OER at 300 K for the NM-doped systems, respectively. In Figure 11 and Table 3, it can be observed that the Si−N2−Pt-doped system has the smallest limiting reaction barrier (i.e., ΔG_{RDS} = 0.87 eV), while the Si−O2−Ir-doped system has the largest limiting reaction barrier (i.e., ΔG_{RDS} = 5.84 eV), which implies that the Si−N2−Pt-doped system has the best OER activity, while the Si−O2−Ir-doped system shows the worst OER performance. In addition, it can also be found in Table 3 that the RDS of the Si−O2−Ru-, Si−O2−Rh-, Si−Se2−Os-, and Si−O2−Ir-doped systems is *OOH → O_2 while that of other NM-doped systems is *O → *OOH.

4. SUMMARY

In summary, we studied the stability of 48 NM-doped systems based on DFT and investigated the electronic properties and water splitting activity of 15 more stable NM-doped systems based on stability. By comparing the binding energies of six NM-doped PM adsorption systems, it can be found that, compared with other NM-doped systems, Si−O2−Ru-, Si−O2−Rh-, Si−N2−Os-, Si−O2−Os-, Si−P2−Os-, Si−S2−Os-, Si−Se2−Os-, Si−N2−Ir-, Si−O2−Ir-, Si−P2− Ir-, Si−S2−Ir-, Si−Se2−Ir-, Si−N2−Pt-, Si−O2−Pt-, and Si−Se2−Pt-doped systems are more stable. Therefore, we carried out a follow-up study with these 15 more stable NM-doped systems as the

https://doi.org/10.1021/acsomega.2c03388
ACS Omega 2022, 7, 33156−33166

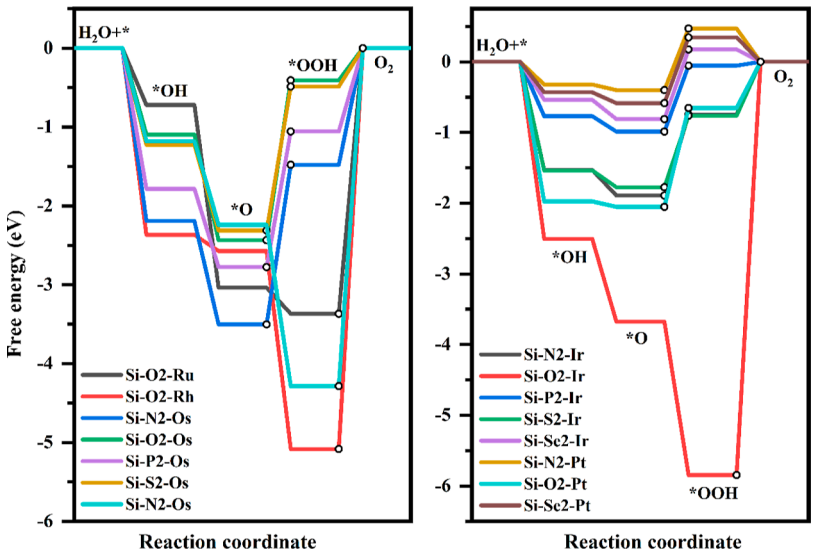

Figure 11. Free-energy diagram at 1.23 eV for the OER over NM-doped systems at 300 K. The two circles represent the RDS.

Table 3. RDS and Limiting Reaction Barrier (ΔG) of the OER over NM-Doped Systems at 300 K

	RDS	ΔG_{RDS} (eV)
Si−O2−Ru	*OOH → O_2	3.37
Si−O2−Rh	*OOH → O_2	5.08
Si−N2−Os	*O → *OOH	2.03
Si−O2−Os	*O → *OOH	2.03
Si−P2−Os	*O → *OOH	1.72
Si−S2−Os	*O → *OOH	1.82
Si−Se2−Os	*OOH → O_2	4.29
Si−N2−Ir	*O → *OOH	1.15
Si−O2−Ir	*OOH → O_2	5.84
Si−P2−Ir	*O → *OOH	0.93
Si−S2−Ir	*O → *OOH	1.01
Si−Se2−Ir	*O → *OOH	0.98
Si−N2−Pt	*O → *OOH	0.87
Si−O2−Pt	*O → *OOH	1.40
Si−Se2−Pt	*O → *OOH	0.93

main study. In addition, based on the binding energy of 48 NM-doped systems, it can also be found that the O2-doped systems are the most stable compared to other NM-doped systems, and the NM-doped Os, Ir, and Pt adsorption systems are more stable. Second, by studying the electronic properties of the 15 more stable NM-doped systems, the following properties can be found: (1) the PM atoms bond with the nearest Si atoms by a mixture of covalent and ionic bonds in Si−O2−Ru-, Si−O2−Rh-, and Si−O2−Ir-doped systems, while PM−Si bonds and PM−NM bonds behave as ionic bonds in the other NM-doped systems; (2) Si−O2−Ru-, Si−N2−Os-, Si−P2−Os-, and Si−O2−Pt-doped systems exhibit semiconductor properties with narrow energy gaps, while other NM-doped systems exhibit metallic properties; (3) Si−O2−Rh-, Si−S2−Ir-, and Si−Se2−Ir-doped systems are magnetic, while other NM-doped systems have no magnetic properties. Finally, the water splitting activities of the 15 more stable NM-doped systems were investigated based on the SHE, and it was found that (1) the HER activities of Si−O2−Pt- and Si−Se2−Pt-doped systems decreased with increasing temperature, while the HER properties of other NM-doped systems increased with increasing temperature; (2) Si−O2−Ir-, Si−O2−Rh-, Si−Se2−Os-, and Si−O2−Ru-doped systems showed enhanced OER activity with increasing temperature, while the OER performance of other NM-doped systems decreased with increasing temperature; (3) the Si−S2−Ir-doped system showed excellent HER performance at 300 K, while the Si−N2−Pt-doped system showed the best OER activity. Our findings provide theoretical support for the application of silicene in the field of electrocatalytic hydrolysis in the future.

■ ASSOCIATED CONTENT

Supporting Information

The Supporting Information is available free of charge at https://pubs.acs.org/doi/10.1021/acsomega.2c03388.

Calculation methods and results, geometric structure of PM-adsorbed silicene with doped NMs; charge density difference for PM-adsorbed silicene with doped NMs; PDOS of PM-adsorbed silicene with doped NMs; and RDS and limiting reaction barrier of OER over NM-doped systems at temperatures between 200 and 600 K (PDF)

■ AUTHOR INFORMATION

Corresponding Author

Yao He − *Department of Physics, Yunnan University, Kunming 650091, China*; Email: yhe@ynu.edu.cn

Authors

Wen-Zhong Li − *Department of Physics, Yunnan University, Kunming 650091, China*; orcid.org/0000-0002-4156-0042

Yong Mao − *Materials Genome Institute, School of Materials and Energy, Yunnan University, Kunming 650091, China*

Kai Xiong − *Materials Genome Institute, School of Materials and Energy, Yunnan University, Kunming 650091, China*

Complete contact information is available at: https://pubs.acs.org/10.1021/acsomega.2c03388

Author Contributions

W.-Z.L.: conceptualization, writing—original draft, data curation, visualization. Y.H.: supervision, methodology. Y.M.: methodology, visualization. K.X.: methodology, visualization.

https://doi.org/10.1021/acsomega.2c03388
ACS Omega 2022, 7, 33156−33166

Notes

The authors declare no competing financial interest.

■ ACKNOWLEDGMENTS

This work was supported by the National Natural Science Foundation of China (grant no. 12164050), Major Science and Technology Project of Precious Metal Materials Genetic Engineering in Yunnan Province (grant nos. 2019ZE001-1, 202002AB080001-6, and 2018IC058), Program for Yunling Scholars in Yunnan Province, Program for Donglu Scholars in Yunnan University, and Project of the Science Research Foundation of the Department of Education in Yunnan Province (grant no. 2022Y052). Computational resources were provided by the Advanced Computing Center of Yunnan University.

■ REFERENCES

(1) Chen, H.; Cong, T. N.; Yang, W.; Tan, C.; Li, Y.; Ding, Y. Progress in Electrical Energy Storage System: A Critical Review. *Prog. Nat. Sci.* **2009**, *19*, 291−312.
(2) Zhu, J.; Hu, L.; Zhao, P.; Lee, L. Y. S.; Wong, K.-Y. Recent Advances in Electrocatalytic Hydrogen Evolution Using Nanoparticles. *Chem. Rev.* **2020**, *120*, 851−918.
(3) Momirlan, M.; Veziroglu, T. N. The Properties of Hydrogen as Fuel Tomorrow in Sustainable Energy System for a Cleaner Planet. *Int. J. Hydrogen Energy* **2005**, *30*, 795−802.
(4) Nørskov, J. K.; Rossmeisl, J.; Logadottir, A.; Lindqvist, L.; Kitchin, J. R.; Bligaard, T.; Jónsson, H. Origin of the Overpotential for Oxygen Reduction at a Fuel-Cell Cathode. *J. Phys. Chem. B* **2004**, *108*, 17886−17892.
(5) Nørskov, J. K.; Bligaard, T.; Logadottir, A.; Kitchin, J. R.; Chen, J. G.; Pandelov, S.; Stimming, U. Trends in the Exchange Current for Hydrogen Evolution. *J. Electrochem. Soc.* **2005**, *152*, J23−J26.
(6) Jiao, Y.; Zheng, Y.; Jaroniec, M.; Qiao, S. Z. Design of Electrocatalysts for Oxygen- and Hydrogen-Involving Energy Conversion Reactions. *Chem. Soc. Rev.* **2015**, *44*, 2060−2086.
(7) Zhang, H.; Nai, J.; Yu, L.; Lou, X. W. D. Metal-Organic-Framework-Based Materials as Platforms for Renewable Energy and Environmental Applications. *Joule* **2017**, *1*, 77−107.
(8) Wang, J.; Cui, W.; Liu, Q.; Xing, Z.; Asiri, A. M.; Sun, X. Recent Progress in Cobalt-Based Heterogeneous Catalysts for Electrochemical Water Splitting. *Adv. Mater.* **2016**, *28*, 215−230.
(9) Zhang, H.; Liu, Y.; Chen, T.; Zhang, J.; Zhang, J.; Lou, X. W. D. Unveiling the Activity Origin of Electrocatalytic Oxygen Evolution over Isolated Ni Atoms Supported on a N-Doped Carbon Matrix. *Adv. Mater.* **2019**, *31*, 1904548.
(10) Zhao, J.; Liu, H.; Yu, Z.; Quhe, R.; Zhou, S.; Wang, Y.; Liu, C. C.; Zhong, H.; Han, N.; Lu, J.; Yao, Y.; Wu, K. Rise of Silicene: A Competitive 2D Material. *Prog. Mater. Sci.* **2016**, *83*, 24−151.
(11) Tang, Q.; Zhou, Z. Graphene-Analogous Low-Dimensional Materials. *Prog. Mater. Sci.* **2013**, *58*, 1244−1315.
(12) Meng, X.; Deng, D. Two-Dimensional Materials for Electrocatalytic Water Splitting. *Chin. Sci. Bull.* **2017**, *62*, 3154−3172.
(13) Pumera, M. Materials Electrochemists' Never-Ending Quest for Efficient Electrocatalysts: The Devil Is in the Impurities. *ACS Catal.* **2020**, *10*, 7087−7092.
(14) Fei, H.; Dong, J.; Feng, Y.; Allen, C. S.; Wan, C.; Volosskiy, B.; Li, M.; Zhao, Z.; Wang, Y.; Sun, H.; An, P.; Chen, W.; Guo, Z.; Lee, C.; Chen, D.; Shakir, I.; Liu, M.; Hu, T.; Li, Y.; Kirkland, A. I.; Duan, X.; Huang, Y. General Synthesis and Definitive Structural Identification of MN4C4 Single-Atom Catalysts with Tunable Electrocatalytic Activities. *Nat. Catal.* **2018**, *1*, 63−72.
(15) Sun, X.; Li, K.; Yin, C.; Wang, Y.; Jiao, M.; He, F.; Bai, X.; Tang, H.; Wu, Z. Dual-Site Oxygen Reduction Reaction Mechanism on CoN4 and CoN2 Embedded Graphene: Theoretical Insights. *Carbon* **2016**, *108*, 541−550.
(16) Li, Q.; Chen, W.; Xiao, H.; Gong, Y.; Li, Z.; Zheng, L.; Zheng, X.; Yan, W.; Cheong, W.-C.; Shen, R.; Fu, N.; Gu, L.; Zhuang, Z.; Chen, C.; Wang, D.; Peng, Q.; Li, J.; Li, Y. Fe Isolated Single Atoms on S, N Codoped Carbon by Copolymer Pyrolysis Strategy for Highly Efficient Oxygen Reduction Reaction. *Adv. Mater.* **2018**, *30*, 1800588.
(17) Kattel, S.; Wang, G. Reaction Pathway for Oxygen Reduction on FeN4 Embedded Graphene. *J. Phys. Chem. Lett.* **2014**, *5*, 452−456.
(18) Yang, T.; Huang, Y.; Yang, L.; Li, X.; Wang, X.; Zhang, G.; Luo, Y.; Jiang, J. Protecting Single Atom Catalysts with Graphene/Carbon-Nitride "Chainmail". *J. Phys. Chem. Lett.* **2019**, *10*, 3129−3133.
(19) Cheng, N.; Stambula, S.; Wang, D.; Banis, M. N.; Liu, J.; Riese, A.; Xiao, B.; Li, R.; Sham, T.-K.; Liu, L.-M.; Botton, G. A.; Sun, X. Platinum Single-Atom and Cluster Catalysis of the Hydrogen Evolution Reaction. *Nat. Commun.* **2016**, *7*, 13638.
(20) Zou, X.; Silva, R.; Goswami, A.; Asefa, T. Cu-Doped Carbon Nitride: Bio-Inspired Synthesis of H2-Evolving Electrocatalysts Using Graphitic Carbon Nitride (g-C3N4) as a Host Material. *Appl. Surf. Sci.* **2015**, *357*, 221−228.
(21) Zhang, X.; Lu, Z.; Yang, Z. Single Non-Noble-Metal Cobalt Atom Stabilized by Pyridinic Vacancy Graphene: An Efficient Catalyst for CO Oxidation. *J. Mol. Catal. A: Chem.* **2016**, *417*, 28−35.
(22) He, B. L.; Shen, J. S.; Tian, Z. X. Iron-Embedded C2N Monolayer: A Promising Low-Cost and High-Activity Single-Atom Catalyst for CO Oxidation. *Phys. Chem. Chem. Phys.* **2016**, *18*, 24261−24269.
(23) Tang, Y.; Zhou, J.; Shen, Z.; Chen, W.; Li, C.; Dai, X. High Catalytic Activity for CO Oxidation on Single Fe Atom Stabilized in Graphene Vacancies. *RSC Adv.* **2016**, *6*, 93985−93996.
(24) Chhowalla, M.; Shin, H. S.; Eda, G.; Li, L.-J.; Loh, K. P.; Zhang, H. The Chemistry of Two-Dimensional Layered Transition Metal Dichalcogenide Nanosheets. *Nat. Chem.* **2013**, *5*, 263−275.
(25) Xie, J.; Zhang, H.; Li, S.; Wang, R.; Sun, X.; Zhou, M.; Zhou, J.; Lou, X. W.D.; Xie, Y. Defect-Rich MoS2Ultrathin Nanosheets with Additional Active Edge Sites for Enhanced Electrocatalytic Hydrogen Evolution. *Adv. Mater.* **2013**, *25*, 5807−5813.
(26) Song, C. An Overview of New Approaches to Deep Desulfurization for Ultra-Clean Gasoline, Diesel Fuel and Jet Fuel. *Catal. Today* **2003**, *86*, 211−263.
(27) Raybaud, P.; Hafner, J.; Kresse, G.; Kasztelan, S.; Toulhoat, H. Structure, Energetics, and Electronic Properties of the Surface of a Promoted MoS2 Catalyst: An Ab Initio Local Density Functional Study. *J. Catal.* **2000**, *190*, 128−143.
(28) Hinnemann, B.; Moses, P. G.; Bonde, J.; Jørgensen, K. P.; Nielsen, J. H.; Horch, S.; Chorkendorff, I.; Nørskov, J. K. Biomimetic Hydrogen Evolution: MoS2 Nanoparticles as Catalyst for Hydrogen Evolution. *J. Am. Chem. Soc.* **2005**, *127*, 5308−5309.
(29) Bonde, J.; Moses, P. G.; Jaramillo, T. F.; Nørskov, J. K.; Chorkendorff, I. Hydrogen Evolution on Nano-Particulate Transition Metal Sulfides. *Faraday Discuss.* **2009**, *140*, 219−231.
(30) Li, Y.; Wang, H.; Xie, L.; Liang, Y.; Hong, G.; Dai, H. MoS2 Nanoparticles Grown on Graphene: An Advanced Catalyst for the Hydrogen Evolution Reaction. *J. Am. Chem. Soc.* **2011**, *133*, 7296−7299.
(31) Lukowski, M. A.; Daniel, A. S.; English, C. R.; Meng, F.; Forticaux, A.; Hamers, R. J.; Jin, S. Highly Active Hydrogen Evolution Catalysis from Metallic WS2 Nanosheets. *Energy Environ. Sci.* **2014**, *7*, 2608−2613.
(32) Voiry, D.; Yamaguchi, H.; Li, J.; Silva, R.; Alves, D. C. B.; Fujita, T.; Chen, M.; Asefa, T.; Shenoy, V. B.; Eda, G.; Chhowalla, M. Enhanced Catalytic Activity in Strained Chemically Exfoliated WS2 Nanosheets for Hydrogen Evolution. *Nat. Mater.* **2013**, *12*, 850−855.
(33) Banhart, F.; Kotakoski, J.; Krasheninnikov, A. V. Structural Defects in Graphene. *ACS Nano* **2011**, *5*, 26−41.
(34) Zhong, J.-H.; Zhang, J.; Jin, X.; Liu, J.-Y.; Li, Q.; Li, M.-H.; Cai, W.; Wu, D.-Y.; Zhan, D.; Ren, B. Quantitative Correlation between Defect Density and Heterogeneous Electron Transfer Rate of Single Layer Graphene. *J. Am. Chem. Soc.* **2014**, *136*, 16609−16617.

https://doi.org/10.1021/acsomega.2c03388
ACS Omega 2022, 7, 33156−33166

(35) Li, L.; Reich, S.; Robertson, J. Defect Energies of Graphite: Density-Functional Calculations. *Phys. Rev. B: Condens. Matter Mater. Phys.* **2005**, *72*, 184109.
(36) Wang, H.; Wang, Q.; Cheng, Y.; Li, K.; Yao, Y.; Zhang, Q.; Dong, C.; Wang, P.; Schwingenschlögl, U.; Yang, W.; Zhang, X. X. Doping Monolayer Graphene with Single Atom Substitutions. *Nano Lett.* **2012**, *12*, 141−144.
(37) Yang, Z.; Yao, Z.; Li, G.; Fang, G.; Nie, H.; Liu, Z.; Zhou, X.; Chen, X.; Huang, S. Sulfur-Doped Graphene as an Efficient Metal-Free Cathode Catalyst for Oxygen Reduction. *ACS Nano* **2012**, *6*, 205−211.
(38) Jiao, Y.; Zheng, Y.; Jaroniec, M.; Qiao, S. Z. Origin of the Electrocatalytic Oxygen Reduction Activity of Graphene-Based Catalysts: A Roadmap to Achieve the Best Performance. *J. Am. Chem. Soc.* **2014**, *136*, 4394−4403.
(39) Panchakarla, L. S.; Subrahmanyam, K. S.; Saha, S. K.; Govindaraj, A.; Krishnamurthy, H. R.; Waghmare, U. V.; Rao, C. N. R. Synthesis, Structure, and Properties of Boron- and Nitrogen-Doped Graphene. *Adv. Mater.* **2009**, *21*, 4726−4730.
(40) Poh, H. L.; Šimek, P.; Sofer, Z.; Pumera, M. Halogenation of Graphene with Chlorine, Bromine, or Iodine by Exfoliation in a Halogen Atmosphere. *Chem.—Eur. J.* **2013**, *19*, 2655−2662.
(41) Liu, F.; Sun, J.; Zhu, L.; Meng, X.; Qi, C.; Xiao, F.-S. Sulfated Graphene as an Efficient Solid Catalyst for Acid-Catalyzed Liquid Reactions. *J. Mater. Chem.* **2012**, *22*, 5495−5502.
(42) Zheng, Y.; Jiao, Y.; Zhu, Y.; Li, L. H.; Han, Y.; Chen, Y.; Du, A.; Jaroniec, M.; Qiao, S. Z. Hydrogen Evolution by a Metal-Free Electrocatalyst. *Nat. Commun.* **2014**, *5*, 3783.
(43) Duan, J.; Chen, S.; Jaroniec, M.; Qiao, S. Z. Porous C3N4Nanolayers@N-Graphene Films as Catalyst Electrodes for Highly Efficient Hydrogen Evolution. *ACS Nano* **2015**, *9*, 931−940.
(44) Chua, X. J.; Luxa, J.; Eng, A. Y. S.; Tan, S. M.; Sofer, Z.; Pumera, M. Negative Electrocatalytic Effects of P-Doping Niobium and Tantalum on MoS2 and WS2 for the Hydrogen Evolution Reaction and Oxygen Reduction Reaction. *ACS Catal.* **2016**, *6*, 5724−5734.
(45) Guo, J.; Zhu, H.; Sun, Y.; Tang, L.; Zhang, X. Doping MoS2 with Graphene Quantum Dots: Structural and Electrical Engineering towards Enhanced Electrochemical Hydrogen Evolution. *Electrochim. Acta* **2016**, *211*, 603−610.
(46) Ma, X.; Li, J.; An, C.; Feng, J.; Chi, Y.; Liu, J.; Zhang, J.; Sun, Y. Ultrathin Co(Ni)-Doped MoS2 Nanosheets as Catalytic Promoters Enabling Efficient Solar Hydrogen Production. *Nano Res.* **2016**, *9*, 2284−2293.
(47) Tang, Q.; Jiang, D. Stabilization and Band-Gap Tuning of the 1T-MoS2 Monolayer by Covalent Functionalization. *Chem. Mater.* **2015**, *27*, 3743−3748.
(48) Zhou, L.; He, B.; Yang, Y.; He, Y. Facile approach to surface functionalized MoS2nanosheets. *RSC Adv.* **2014**, *4*, 32570−32578.
(49) Ouyang, Y.; Ling, C.; Chen, Q.; Wang, Z.; Shi, L.; Wang, J. Activating Inert Basal Planes of MoS2for Hydrogen Evolution Reaction through the Formation of Different Intrinsic Defects. *Chem. Mater.* **2016**, *28*, 4390−4396.
(50) Yin, Y.; Han, J.; Zhang, Y.; Zhang, X.; Xu, P.; Yuan, Q.; Samad, L.; Wang, X.; Wang, Y.; Zhang, Z.; Zhang, P.; Cao, X.; Song, B.; Jin, S. Contributions of Phase, Sulfur Vacancies, and Edges to the Hydrogen Evolution Reaction Catalytic Activity of Porous Molybdenum Disulfide Nanosheets. *J. Am. Chem. Soc.* **2016**, *138*, 7965−7972.
(51) Li, S.; Ren, J.-C.; Ao, Z.; Liu, W. Enhanced Stability and Induced Magnetic Moments of Silicene by Substitutional Doping of Nickel. *Chem. Phys. Lett.* **2018**, *706*, 202−207.
(52) Sahin, H.; Peeters, F. M. Adsorption of alkali, alkaline-earth, and 3dtransition metal atoms on silicene. *Phys. Rev. B: Condens. Matter Mater. Phys.* **2013**, *87*, 85423.
(53) Zheng, R.; Lin, X.; Ni, J. The Extraordinary Magnetoelectric Response in Silicene Doped with Fe and Cr Atoms. *Appl. Phys. Lett.* **2014**, *105*, 092410.
(54) Zheng, R.; Chen, Y.; Ni, J. Highly Tunable Magnetism in Silicene Doped with Cr and Fe Atoms under Isotropic and Uniaxial Tensile Strain. *Appl. Phys. Lett.* **2015**, *107*, 263104.
(55) Lin, X.; Ni, J. Much Stronger Binding of Metal Adatoms to Silicene than to Graphene: A First-Principles Study. *Phys. Rev. B: Condens. Matter Mater. Phys.* **2012**, *86*, 75440.
(56) Ersan, F.; Arslanalp, Ö.; Gökoğlu, G.; Aktürk, E. Effect of Adatoms and Molecules on the Physical Properties of Platinum-Doped and -Substituted Silicene: A First-Principles Investigation. *Appl. Surf. Sci.* **2016**, *371*, 314−321.
(57) Li, W.-Z.; Liu, M.-Y.; Gong, L.; Zhang, M.-L.; Cao, C.; He, Y. The Electronic Properties and Catalytic Activity of Precious-Metals Adsorbed Silicene for Hydrogen Evolution Reaction and Oxygen Evolution Reaction. *Appl. Surf. Sci.* **2021**, *560*, 150041.
(58) Ma, L.; Zhang, J.-M.; Xu, K.-W.; Ji, V. Nitrogen and Boron Substitutional Doped Zigzag Silicene Nanoribbons: Ab Initio Investigation. *Phys. E* **2014**, *60*, 112−117.
(59) Hernández Cocoletzi, H.; Castellanos Águila, J. E. DFT Studies on the Al, B, and P Doping of Silicene. *Superlattices Microstruct.* **2018**, *114*, 242−250.
(60) Jose, D.; Datta, A. Understanding of the Buckling Distortions in Silicene. *J. Phys. Chem. C* **2012**, *116*, 24639−24648.
(61) Jose, D.; Datta, A. Structures and Chemical Properties of Silicene: Unlike Graphene. *Acc. Chem. Res.* **2014**, *47*, 593−602.
(62) Pratik, S. Md.; Nijamudheen, A.; Datta, A. Topochemical Transformations of CaX2(X=C, Si, Ge) to Form Free-Standing Two-Dimensional Materials. *Chem.—Eur. J.* **2015**, *21*, 18454−18460.
(63) Gablech, I.; Pekárek, J.; Klempa, J.; Svatoš, V.; Sajedi-Moghaddam, A.; Neužil, P.; Pumera, M. Monoelemental 2D Materials-Based Field Effect Transistors for Sensing and Biosensing: Phosphorene, Antimonene, Arsenene, Silicene, and Germanene Go beyond Graphene. *TrAC, Trends Anal. Chem.* **2018**, *105*, 251−262.
(64) Chia, H. L.; Sturala, J.; Webster, R. D.; Pumera, M. Functionalized 2D Germanene and Silicene Enzymatic System. *Adv. Funct. Mater.* **2021**, *31*, 2011125.
(65) Hohenberg, P.; Kohn, W. Inhomogeneous Electron Gas. *Phys. Rev.* **1964**, *136*, B864−B871.
(66) Kohn, W.; Sham, L. J. Self-Consistent Equations Including Exchange and Correlation Effects. *Phys. Rev.* **1965**, *140*, A1133−A1138.
(67) Kresse, G.; Furthmüller, J. Efficient iterative schemes forab initiototal-energy calculations using a plane-wave basis set. *Phys. Rev. B: Condens. Matter Mater. Phys.* **1996**, *54*, 11169−11186.
(68) Kresse, G.; Furthmüller, J. Efficiency of Ab-Initio Total Energy Calculations for Metals and Semiconductors Using a Plane-Wave Basis Set. *Comput. Mater. Sci.* **1996**, *6*, 15−50.
(69) Blöchl, P. E. Projector Augmented-Wave Method. *Phys. Rev. B: Condens. Matter Mater. Phys.* **1994**, *50*, 17953−17979.
(70) Perdew, J. P.; Burke, K.; Ernzerhof, M. Generalized Gradient Approximation Made Simple. *Phys. Rev. Lett.* **1996**, *77*, 3865−3868.
(71) Wang, V.; Xu, N.; Liu, J.-C.; Tang, G.; Geng, W.-T. VASPKIT: A User-Friendly Interface Facilitating High-Throughput Computing and Analysis Using VASP Code. *Comput. Phys. Commun.* **2021**, *267*, 108033.
(72) Momma, K.; Izumi, F. VESTA 3 for Three-Dimensional Visualization of Crystal, Volumetric and Morphology Data. *J. Appl. Crystallogr.* **2011**, *44*, 1272−1276.
(73) Dudarev, S. L.; Botton, G. A.; Savrasov, S. Y.; Humphreys, C. J.; Sutton, A. P. Electron-Energy-Loss Spectra and the Structural Stability of Nickel Oxide: An LSDA+U Study. *Phys. Rev. B: Condens. Matter Mater. Phys.* **1998**, *57*, 1505−1509.
(74) Cococcioni, M.; de Gironcoli, S. Linear response approach to the calculation of the effective interaction parameters in theLDA +Umethod. *Phys. Rev. B: Condens. Matter Mater. Phys.* **2005**, *71*, 35105.
(75) Liu, X.; Duan, T.; Meng, C.; Han, Y. Pt Atoms Stabilized on Hexagonal Boron Nitride as Efficient Single-Atom Catalysts for CO Oxidation: A First-Principles Investigation. *RSC Adv.* **2015**, *5*, 10452−10459.

https://doi.org/10.1021/acsomega.2c03388
ACS Omega 2022, 7, 33156−33166

(76) Du, C.; Lin, H.; Lin, B.; Ma, Z.; Hou, T.; Tang, J.; Li, Y. MoS2 Supported Single Platinum Atoms and Their Superior Catalytic Activity for CO Oxidation: A Density Functional Theory Study. *J. Mater. Chem. A* **2015**, *3*, 23113−23119.
(77) Sun, M.; Ren, Q.; Wang, S.; Zhang, Y.; Du, Y.; Yu, J.; Tang, W. Magnetism in Transition-Metal-Doped Germanene: A First-Principles Study. *Comput. Mater. Sci.* **2016**, *118*, 112−116.
(78) Kaloni, T. P. Tuning the Structural, Electronic, and Magnetic Properties of Germanene by the Adsorption of 3d Transition Metal Atoms. *J. Phys. Chem. C* **2014**, *118*, 25200−25208.
(79) Cahangirov, S.; Topsakal, M.; Aktürk, E.; Şahin, H.; Ciraci, S. Two- and One-Dimensional Honeycomb Structures of Silicon and Germanium. *Phys. Rev. Lett.* **2009**, *102*, 236804.
(80) Deng, D.; Yu, L.; Chen, X.; Wang, G.; Jin, L.; Pan, X.; Deng, J.; Sun, G.; Bao, X. Iron Encapsulated within Pod-like Carbon Nanotubes for Oxygen Reduction Reaction. *Angew. Chem., Int. Ed.* **2013**, *52*, 371−375.

https://doi.org/10.1021/acsomega.2c03388
ACS Omega 2022, 7, 33156−33166